

EXPERIMENTAL STUDY ON INFRARED THERMAL WAVE DETECTION OF HONEYCOMB SANDWICH STRUCTURE DEFECTS BY USING BARKER CODE EXCITATION

by

**Qing-Ju TANG^{a*}, Hong-Ru BU^a, Zhuo-Yan GU^b, Hao-Dong LI^a,
Rui XIE^a, Vladimir VAVILOV^c, and Arsenii CHULKOV^c**

^a School of Mechanical Engineering,
Heilongjiang University of Science and Technology, Harbin, China

^b School of Safety Engineering,
Heilongjiang University of Science and Technology, Harbin, China

^c Engineering School of NDT, Tomsk Polytechnic University, Tomsk, Russia

Original scientific paper
<https://doi.org/10.2298/TSCI2502273T>

The paper describes a thermal testing system implementing Barker code thermal wave excitation accurately detect defects in GFRP/NOMEX honeycomb sandwich structures. Influence of defect parameters on detection efficiency is explored. Four algorithms, namely, PCA, PPT, THD, and TW-PCA, have been used to process infrared image sequences. The obtained results show that all algorithms suppress background noise to a certain degree, but the TW-PCA technique has proven to be more effective providing the higher both signal-to-noise ratio and information entropy.

Key words: *GFRP/NOMEX honeycomb sandwich structure, signal-to-noise ratio, barker code excitation, image sequence processing, information entropy*

Introduction

The GFRP/NOMEX honeycomb sandwich structures are widely used in the aerospace and other fields due to their high thermal and sound insulation properties [1]. However, due to the complex manufacturing process and harsh operating conditions, such structures are prone to delaminations and debonding defects [2]. Infrared (IR) thermal wave non-destructive testing (NDT) offers an intuitive, fast, efficient and non-contact inspection technique, making it ideal for identifying defects in GFRP/NOMEX honeycomb sandwich structures [3]. In its turn, the Barker code, that is a key two-phase code in radar systems, features ideal autocorrelation and excellent pulse compression properties [4].

Technology for detecting infrared thermal waves using Barker code excitation

A Barker code sequence is characterized by an ideal aperiodic autocorrelation function:

$$R(m) = \sum_{k=0}^{N-1-|m|} c_k c_{k+m} = \begin{cases} N, & m = 0 \\ 0 \text{ or } \pm 1, & m \neq 0 \end{cases} \quad (1)$$

where N is the code length.

At present, seven different lengths of Barker codes ($N=2, 3, 4, 5, 7, 11,$ and 13) are known.

* Corresponding author, e-mail: tangqingju@126.com

Among all Barker codes, the 13-bit code provides the highest main-to-sidelobe ratio and a wider frequency band, making it ideal for detecting low power signals. Figure 1 presents the schematic diagram of the modulated thermal wave and thermal NDT system.

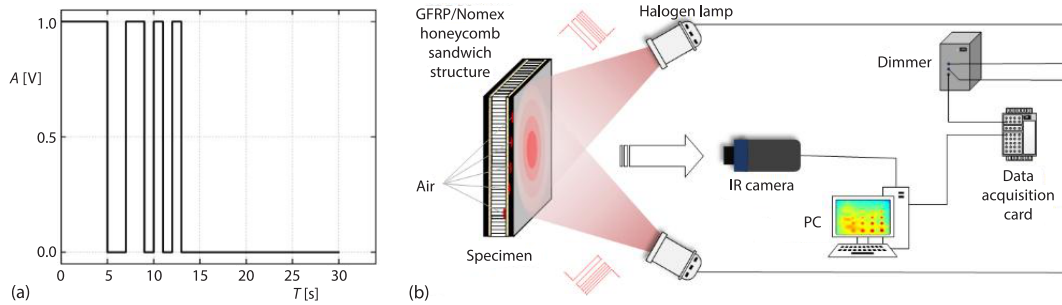


Figure 1. Schematic diagram of modulated thermal wave and detection system;
(a) 13-bit Barker code-modulated thermal wave and (b) experimental thermal NDT system

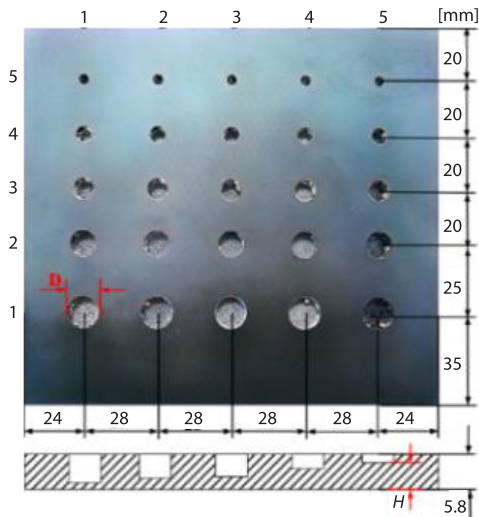


Figure 2. Defect location diagram

where defects with greater diameters and shallower depths provide higher temperature differences, thus making defect detection easier.

Image sequence processing

Principal component analysis

The principal component analysis (PCA) is the process of transforming data to reduce its dimensionality that is often used in the extraction of defect features [5]. The PCA mathematical model [6]:

$$\begin{bmatrix} Z_1 \\ Z_2 \\ \dots \\ Z_M \end{bmatrix} = \begin{bmatrix} b_{11} & b_{12} & \dots & b_{1N} \\ b_{21} & b_{22} & \dots & b_{2N} \\ \dots & \dots & \dots & \dots \\ b_{M1} & b_{M2} & \dots & b_{MN} \end{bmatrix} \begin{bmatrix} x_1 \\ x_2 \\ \dots \\ x_N \end{bmatrix} \tag{2}$$

where Z_m is the m^{th} principal component, x_N – the common factor, and b_{ij} – the feature vector.

Experimental investigation

Test specimen

The specimen dimensions were 140 mm × 160 mm × 5.8 mm with the location of the defects shown in fig. 2.

Experimental parameters

A 13-bit Barker code-modulated pulse excitation has been used (30 seconds acquisition time, 2000 W excitation power and 20 Hz acquisition frequency).

Experimental results and analysis

To study the influence of defect diameter and depth on surface temperature differentials, a couple of temperature profiles have been obtained, fig. 3. As expected, the defects with great-

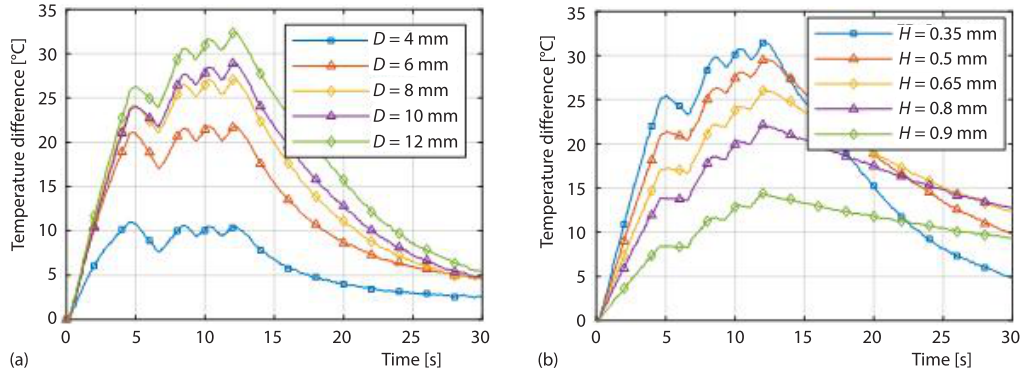


Figure 3. Influence of defect geometric characteristics on surface temperature differentials; (a) defect diameter influence and (b) defect depth influence

Since the eigenvalues $\lambda_1 \geq \lambda_2 \geq \lambda_3 \geq \dots \lambda_k$ of the correlation coefficient matrix are determined, the cumulative contribution rate can be obtained:

$$L = \sum_{m=1}^M \left(\frac{\lambda_m}{\sum_{n=1}^N \lambda_n} \right) \quad (3)$$

As the contribution rate increases, the information on defects becomes more detailed. When the cumulative contribution rate of m primary components exceeds 85%, most of the important characteristics are retrieved [7]. The cumulative contribution rate of the first two principal components exceeds 85%, *i.e.* in this case most of the effective information has been extracted. Figure 4 shows the results obtained with PCA1 and PCA2 to illustrate that this kind of data processing better displays defect features and contours thus improving image quality.

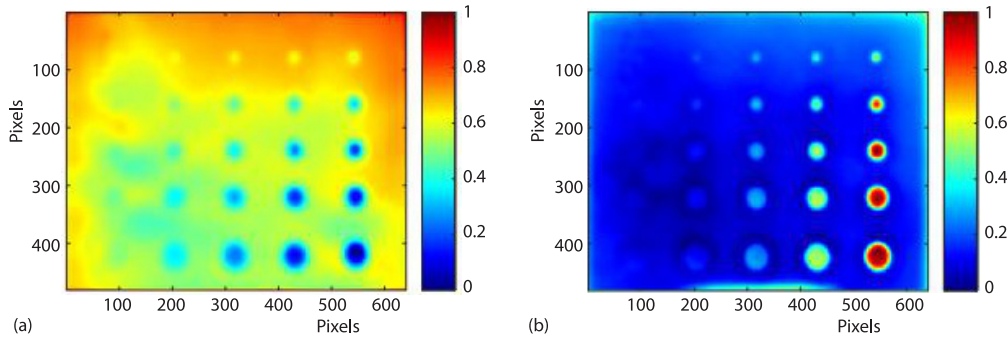


Figure 4. Processing thermal NDT results by using PCA; (a) PCA 1 and (b) PCA 2

Pulse phase thermography

The pulse phase thermography (PPT) is an IR image processing algorithm that includes both the pulse and phase-locked methods [8]. It extracts signals of different frequencies using the Fourier transform spectrum analysis [9]. The relevant formula:

$$F(n) = \sum_{x=0}^{N-1} T(k\Delta t) \exp\left(\frac{-j2\pi nm}{N}\right) = S(n) + jL(n) \quad (4)$$

where $S(n)$ and $L(n)$ are the real and imaginary parts of the frequency domain signals, respectively.

Then the amplitude and phase of the signal are obtained as [10]:

$$A(n) = \sqrt{S(n)^2 + L(n)^2} \quad (5)$$

$$\varphi(n) = \tan^{-1}\left(\frac{L(n)}{S(n)}\right) \quad (6)$$

The PPT result is shown in fig. 5. The amplitude image clearly reveals defect characteristics with a higher contrast and less noise. However, the phase image contains significant background noise and does not distinctly show the defects in the first right column.

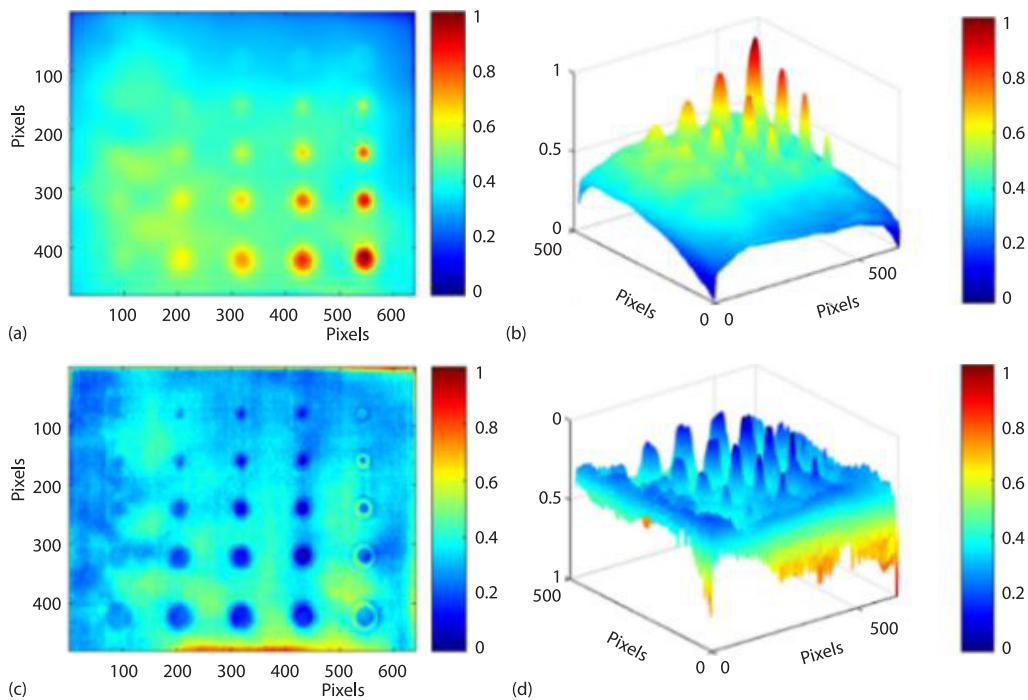


Figure 5. Processing thermal NDT results by using PPT in 2-D and 3-D presentations; (a) and (b) amplitude images and (c) and (d) phase images

Total harmonic distortion

The total harmonic distortion (THD) is an image processing method evaluating the ratio between harmonic and fundamental components in a signal. In IR thermal wave NDT, this approach often provides a more accurate temperature response:

$$\Delta T_{\text{surf}}(t) = \frac{q_0}{e\sqrt{\pi t}} \quad (7)$$

The ratio between the fundamental power and the total harmonic power is [11]:

$$THD_p = \frac{\sum_{n=2}^{\infty} P_n}{P_1} = \frac{\sum_{n=2}^{\infty} V_n^2}{V_1^2} \quad (8)$$

Another method to describe signal harmonic distortion is to determine the amplitude ratio:

$$THD_A = \frac{\sqrt{\sum_{n=2}^{\infty} V_n^2}}{V_1} \quad (9)$$

and then apply the Laplace transform to eq. (9):

$$F_{\text{peak}} = F(s) = \left(\frac{q_0}{e\sqrt{\pi}} \right) \left[\frac{\Gamma(0.5)}{\sqrt{s}} \right] \quad (10)$$

The THD result is presented in fig. 6 to show that the peak image contains a lot of background noise. The signal-to-noise ratio (SNR) image clearly displays the defect contour, but there is a significant distortion of the actual size of the defects and their temperature indications in the 4th column of the defects. In the amplitude and power ratio images, the edges of the defects are blurred thus resulting in poor indications of defect features.

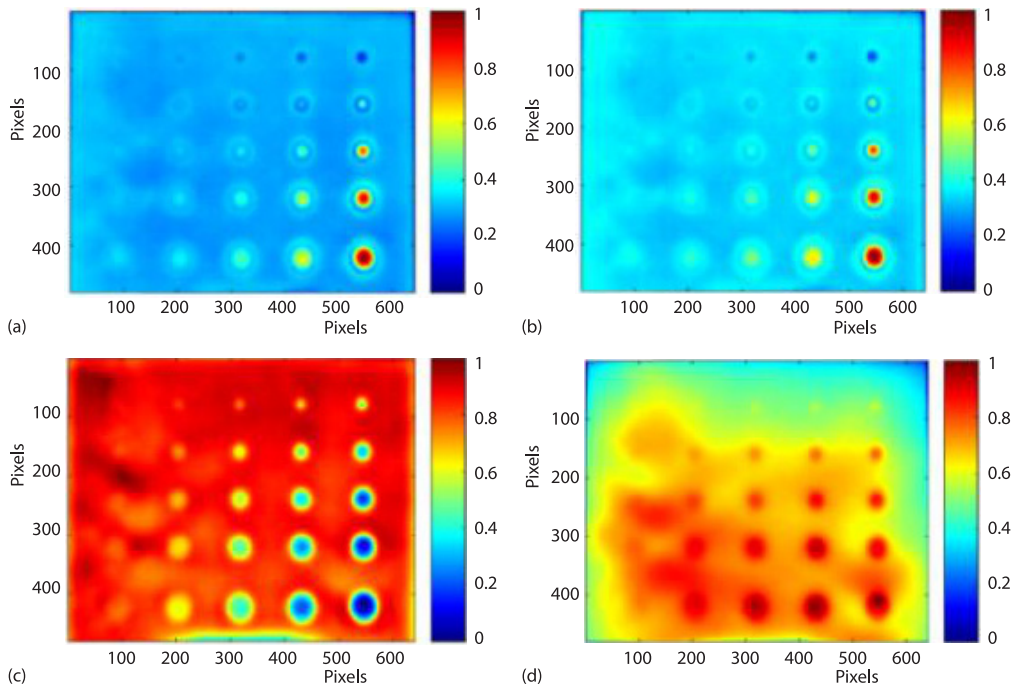


Figure 6. Processing thermal NDT results by using THD; (a) F_{peak} , (b) SNR, (c) THD_A , and (d) THD_P

Temperature-weighted principal component analysis

The temperature-weighted principal component analysis (TW-PCA) optimizes principal component extraction by analyzing temperature variations. Unlike traditional PCA, this algorithm weights inter-frame temperature changes:

$$C = \frac{1}{N} \sum_{i=1}^N \omega_i (x_i - \mu)(x_i - \mu)^T \quad (11)$$

where x_i is the i^{th} data point, μ – the data average value, and ω_i – the weight of the i^{th} data point.

The results of TW-PCA presented in fig. 7 clearly show the defect contours and provide better image contrast and quality.

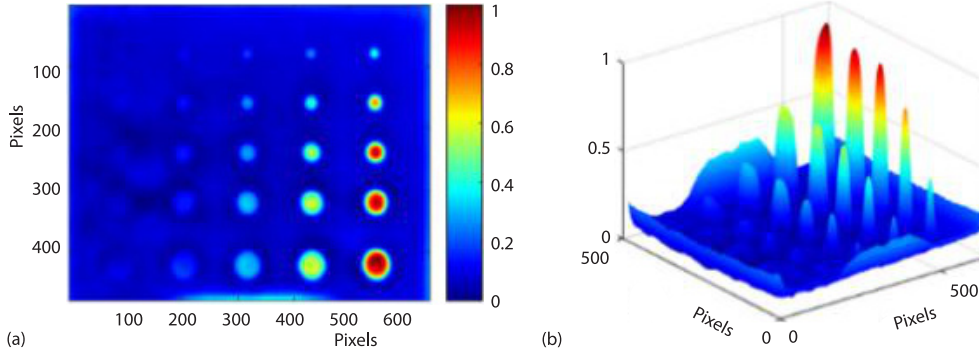


Figure 7. Processing thermal NDT results by using TW-PCA; (a) 2-D graph and (b) 3-D graph

To compare efficiency of aforementioned algorithms, the best resulting images produced by each approach have been evaluated by applying the following figures of merit: SNR and information entropy (IE). The SNR formula:

$$SNR = \frac{|\overline{P_d} - \overline{P_s}|}{\sigma_s} \tag{12}$$

where $\overline{P_d}$ is the average value of the eigenvalues in the defect area, $\overline{P_s}$ – the average of the eigenvalues in the defect-free area, and σ_s – the variance of the eigenvalues in the defect-free area.

Comparative evaluation of the data processing algorithms

In its turn, the IE increases with more information related to the images analyzed, including information on defect indications. The IE formula:

$$IE = -\sum_{n=1}^N [E_n(i, j) \log_2 E_n(i, j)] \tag{13}$$

where $E_n(i, j)$ is the frequency of the gray level signal at the (i, j) image point and $\log_2 E_n(i, j)$ – the logarithm of the gray value frequency.

The SNR and IE values related to the best images derived by the previous techniques have been calculated. Figure 8 shows the chosen reference regions and evaluation indicator results.

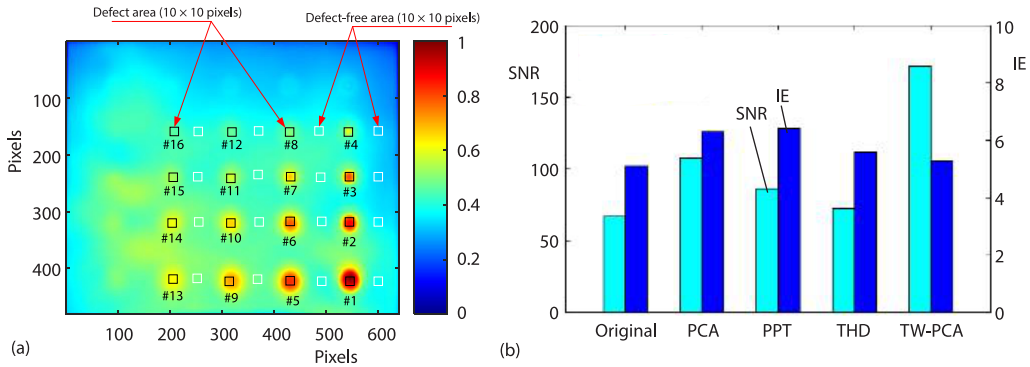


Figure 8. Reference regions and evaluation indicator results; (a) reference regions and (b) SNR and IE values produced by different processing algorithms

It follows from fig. 8 that the TW-PCA technique ensures the highest values of both SNR and IE, making it the preferable method for processing Barker code-generated IR thermal wave images.

Conclusion

Defects in GFRP/NOMEX honeycomb sandwich structures have been identified by using Barker code-modulated IR thermal waves. It has been proven experimentally that inspection efficiency decreases with smaller defect size and greater defect depth. The techniques of PCA, PPT, THD, and TW-PCA have been applied to process test results, with TW-PCA providing the best noise suppression and defect feature extraction.

Acknowledgment

This project is supported by Natural Science Foundation of Heilongjiang Province (Grant No. JQ2023E011) and partially by the FSWW-2023-0004 project of the Ministry of Science and Higher Education of the Russian Federation.

Nomenclature

P_n – power of the n^{th} harmonic, [W]
 q_0 – energy absorbed by the surface, [J]

V_n – voltage of the n^{th} harmonic, [V]
 e – thermal inertia parameters, [$\text{ms}^{-1/2}$]

References

- [1] Fang, W. M., Research on the Technology of GFRP/NOMEX Honeycomb Sandwich Structure Defects Detection Using Infrared Thermal Wave Testing Method (in Chinese), M. Sc. thesis, Heilongjiang University of Science and Technology, Harbin, China, 2022
- [2] Tang, Q. J., et al., Infrared Thermal Imaging Detection and Defect Classification of Honeycomb Sandwich Structure Defects (in Chinese), *Infrared and Laser Engineering*, 53 (2024), 3, pp. 80-91
- [3] Zheng, K., et al., Infrared thermography NDT and Its Development (in Chinese), *Infrared Technology*, 40 (2018), 5, pp. 401-411
- [4] Shi, Q. Z., et al., A Barker-Coded Thermal Wave Imaging for Defect Detection of CFRP Laminate (in Chinese), *Proceedings*, Far East Forum on Non-Destructive Testing New Technology, Xiaman, China, 2018, pp. 470-475
- [5] Luo Y., et al., A Novel Fusion Method of PCA and LDP for Facial Expression Feature Extraction, *Optik*, 127 (2016), 2, pp. 718-721
- [6] Tang, Q. J., et al., A New Signal Processing Algorithm of Pulsed Infrared Thermography, *Infrared Physics & Technology*, 68 (2015), 2, pp. 173-178
- [7] Bu, C. W., et al., Debonding Defects Detection of FML Based on Long Pulsed Infrared Thermography Technique, *Infrared Physics & Technology*, 104 (2020), 2, pp. 124-137
- [8] Yu, J. J., et al., FRP Depth Measurement Based on Pulsed Phase Thermography (in Chinese), *Infrared and Laser Engineering*, 41 (2012), 7, pp. 1893-1898
- [9] Qu, Z., et al., Development and Application of Infrared Thermography Non-Destructive Testing Techniques, *Sensors*, 20 (2020), 2, ID14
- [10] Chen, W. G., et al., A Class of Improved Infrared Non-Destructive Testing Technology for Thermal Wave Image Sequence Processing (in Chinese), *Machine Design and Manufacturing Engineering*, 47 (2018), 12, pp. 101-106
- [11] Larsen, C. A., Document Flash Thermography, M. Sc. thesis, Utah State University, Logan, Ut., USA, 2011